A Battery Management System for Efficient Adherence to Energy Exchange Commands under Longevity Constraints

Mario Vašak†, Goran Kujundžić*
University of Zagreb, Faculty of Electrical Engineering and Computing, Laboratory for Renewable Energy Systems, Unska 3, HR-10000 Zagreb, Croatia,
Public Enterprise Croatian Telecom JSC, Kneza Branimira bb, 88000 Mostar, Bosnia and Herzegovina.
Email: †mario.vasak@fer.hr, *goran.kujundzic@hteronet.ba

***Abstract*—The paper is focussed on the problem of controlling the energy storage such that the energy exchange between the storage and the remaining system is performed in the required amount with maximum efficiency and that all the constraints for the storage system longevity are adhered to. There is a huge need for such a storage management in energy flow optimization of microgrids where energy flows from/to storages are planned in order to achieve maximum gain in microgrid operation. The case of a valve-regulated lead-acid battery is elaborated. The underlying computation tractability and performance of such a battery management system is demonstrated both in simulation and experimentally.**

***Index Terms*—energy storage, energy flow command, constraints, predictive control, optimization, valve-regulated lead-acid battery, energy flow optimization in microgrids**

I. Introduction

Microgrids have operational flexibilities to fulfil system reliability and power quality requirements and also offer possibilities for optimizing distributed generation and improving the energy cost for supplying local loads as shown in [1], [2]. In microgrids the energy generated near the loads can be optimally managed according to different criteria which may in turn increase reliability of local power supply and at the same time reduce losses over long power distribution lines [3].

Energy storage devices are used in microgrids to substantiate these features. They can be various: batteries, supercapacitors, flywheels, hydrogen tanks, compressed air energy storage and others [4], [5]. All of them have operational constraints provided by the manufacturer that need to be respected in order to achieve their longevity. Batteries are common energy storage parts of microgrids and they can ensure a substantial support to microgrid efficient operation as shown in [6], [7]. Charging and discharging of batteries have a significant impact on their lifetime. When the batteries are not properly controlled their significant damage may occur, e.g., water loss, grid corrosion and sulfation of the negative electrode for the case of lead-acid batteries as presented in [8]. Battery manufacturers provide the operational battery constraints during the charging/discharging: the upper and lower voltage level, the maximum charging and discharging currents, the upper and lower state of charge (SOC) level [9], [10]. By retaining the battery states and inputs within the aforementioned operational constraints, the charging and discharging of the batteries will mildly affect their lifetime as shown in [11], [12]. Also, the time and efficiency of battery charging and discharging are important parameters for a better batteries performance in microgrids.

The main level of optimization in microgrids is energy flows optimization. It focusses on planning how much energy needs to be exerted or inserted in a defined amount of time from a microgrid element such as energy storage in order to achieve maximum benefit for the microgrid operation [13], [14]. The current algorithms of energy flow optimization in microgrids lack information which energy flows can be achieved between the microgrid and its energy storage devices such that all longevity constraints are adhered to. Residual SOC is modelled with a constant charging/discharging efficiency model [15]–[17] that introduces significant prediction errors for a broader range of charging/discharging currents needed for highly dynamic battery and microgrid operation. Furthermore, the battery operation to achieve the required energy exchange is not performed in the most energy-efficient way. Thus, the current energy flow optimization algorithms use a microgrid with its battery storage units either conservatively or they command the energy flows whose implementation violates the longevity constraints and strongly negatively affects their state of health (SOH) [18], [19].

It is largely neglected in the literature how the battery should be controlled to yield the commanded energy exchange in the given time. In such a situation the optimization algorithms in charge for the microgrid energy flows optimization lack a proper optimization counterpart on the battery storage system level which would inform (i) about the available charging/discharging energies that can be fulfilled without violating any constraints and (ii) about the optimal residual state of charge related to them. Currently only constant current or constant power schemes are applied when batteries are charged/discharged in microgrids [20]. As a first step in filling this identified gap, design of systematic storage management procedures for efficient adherence to energy exchange commands under longevity constraints is required.

In this paper the storage management system that is subordinated to the microgrid energy flow optimization is presented.

The energy flow optimization yields an energy flow command towards the subordinated management systems of individual storage devices. The paper proposes a storage management procedure based on an optimal control paradigm for efficient adherence to the issued energy exchange commands. The presented storage management retains the states and inputs of energy storage devices within the longevity constraints provided by the manufacturer in order to reduce their degradation effects and prolong their lifetime. The maximal efficiency is formulated with respect to as high as possible residual SOC available after the required amount of energy is exchanged between the storage and the remaining part of the system (microgrid) in the given amount of time. Additionally, the variable efficiency of the charging/discharging depending on charge/discharge energies is incorporated in the system model used for the storage management and thus inherently taken into account.

After presenting the method for solving the posed optimization problem, its application within a closed-loop feedback control system for adherence to energy exchange commands is shown. Closed-loop control enables to perform the exactly required energy exchange in the presence of various disturbances and the model inaccuracies of the storage devices.

Insofar storage management systems in microgrids reduce to maintaining the power output of the storage power converter constant, at the level required by the superimposed microgrid energy flows optimization system [15]–[19]. Such approaches boil down to constant storage power output and, as elaborated before, the longevity constraints of energy storage devices and their variable efficiencies depending on charge/discharge powers are neglected. The approach proposed in this paper can be adjusted to ensure constant power of the power converter while in advance the feasible constant powers can be computed and also the residual SOC accurately predicted for such powers. In addition, by assuming constant power converter losses, the scheme proposed here can be exactly used in ensuring correct energy exchanged with the storage power converter. Closed-loop control would also in this case ensure accurate delivery of the required energy in time even in the case of inaccurately modelled power converter losses.

This paper is focused on valve-regulated lead-acid (VRLA) batteries which are still the optimal choice for microgrids considering price and service life as shown in [21], [22]. Investigation of possibilities of adherence to energy flow commands was initiated in [23] whereas optimization was performed via simulation-based off-line analysis. Here these optimizations are replaced with a systematic approach based on convex and gradient-based constrained optimization that enables real-time operation of such a battery management system.

This paper is organized as follows. Section II presents the main functions of the battery management system and the hybrid electrical model of a VRLA battery. Section III presents the open-loop optimization problem for the proposed battery management with the corresponding algorithms for its solving, while Section IV describes the closed-loop control algorithm under operational constraints with enforced adherence to the commanded energy exchange. Simulation and then experimental results are shown in Section V to validate the performance of the derived battery management system. Section VI concludes the paper.

II. Battery Management System in a Microgrid and the Considered Battery Model

Figure 1 shows a schematic diagram of energy flows optimization in a grid-connected microgrid. Its storage management systems including the Battery Management System (BMS) are subordinated to the microgrid energy flows optimization [23], [24].

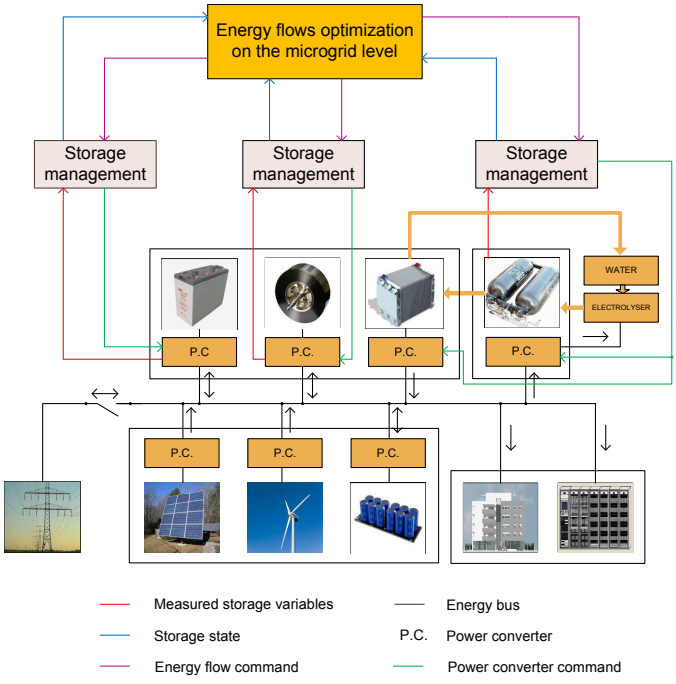

Fig. 1. A schematic diagram of the interaction between energy flows optimization and individual storages management in a microgrid [23]

The BMS manages the conditions of the battery during the charging and discharging in the amounts required by microgrid energy flows optimization, in order to prolong its lifetime. In addition, the other main goal of the BMS is accurate estimation of the battery SOC [25] such that it can be used locally and provided to other system parts, e.g. to energy flows optimization.

In this paper the hybrid electrical model of a battery [26] is used and in the sequel it will be briefly introduced. Self-consumption of the power converter between the microgrid and the battery is neglected.

A. Hybrid electrical model of a VRLA battery

Hybrid electrical model of a battery [26] is shown in Fig. 2 and consists of a capacitor (C_{capacity}) and a current-controlled current source which models the battery SOC. It is an intuitive, accurate and comprehensive electrical battery model and contains an RC network similarly to Thevenin-based models, which is used for modelling the transient response of the

battery. A voltage-controlled voltage source is used to connect SOC to an open-circuit voltage ($V_{\rm OC}$) as described in [27]. In order to model the self-discharging of the battery, an additional leakage resistor ($R_{\rm self}$) can be used in the battery model.

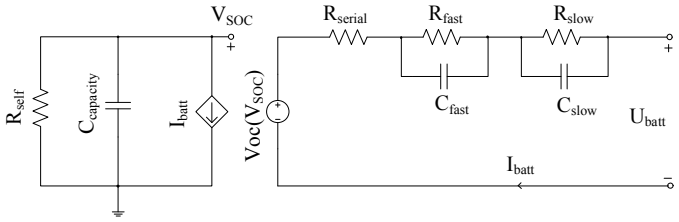

Fig. 2. Hybrid electrical model of a battery [26]

The charge in the capacitor of capacitance $C_{\rm capacity}$ represents the whole charge stored in the battery, i.e. the battery SOC. The capacity of the battery depends on the number of charge/discharge cycles, battery current, ambient temperature and the storage time [28], [29].

In general, the battery SOC has a non-linear dependence on the open-circuit voltage. However, in the case of VRLA batteries authors in papers [30], [31] have shown the linear relationship between the open-circuit voltage and battery SOC. This relationship is based on measuring open-circuit voltage after about 30 minutes of resting period at the different SOC points. Considering this, in this paper a linear approximation for this dependence is used and can be presented as follows:

$$SOC(k) = \frac{100}{a} V_{\rm OC}(k) - \frac{100b}{a}, \tag{1}$$

where b is the open-circuit voltage of an empty battery, while $a+b$ is the open-circuit voltage of a full battery. The open-circuit voltage ($V_{\rm OC}$) is the battery state and in this paper all SOC constraints are formulated through constraints on $V_{\rm OC}$.

The self-discharging of a battery can be neglected due to high values of resistor $R_{\rm self}$ and the hybrid electrical model, shown in Fig. 2, can be presented with the following continuous-time state-space model:

$$\begin{bmatrix} \dot{V}_{\rm OC} \\ \dot{V}_{\rm fast} \\ \dot{V}_{\rm slow} \end{bmatrix} = \begin{bmatrix} 0 & 0 & 0 \\ 0 & \frac{-1}{R_{\rm fast}C_{\rm fast}} & 0 \\ 0 & 0 & \frac{-1}{R_{\rm slow}C_{\rm slow}} \end{bmatrix} \begin{bmatrix} V_{\rm OC} \\ V_{\rm fast} \\ V_{\rm slow} \end{bmatrix} + \begin{bmatrix} \frac{-a}{C_{\rm capacity}} \\ \frac{1}{C_{\rm fast}} \\ \frac{1}{C_{\rm slow}} \end{bmatrix} I_{\rm batt}. \tag{2}$$

Additionally, using the Euler-forward discretization with the sampling time T, the hybrid electric model can be described as the following discrete-time state-space model:

$$\begin{bmatrix} V_{\rm OC}(k+1) \\ V_{\rm fast}(k+1) \\ V_{\rm slow}(k+1) \end{bmatrix} = \begin{bmatrix} 1 & 0 & 0 \\ 0 & 1-\frac{T}{R_{\rm fast}C_{\rm fast}} & 0 \\ 0 & 0 & 1-\frac{T}{R_{\rm slow}C_{\rm slow}} \end{bmatrix} \begin{bmatrix} V_{\rm OC}(k) \\ V_{\rm fast}(k) \\ V_{\rm slow}(k) \end{bmatrix} + \begin{bmatrix} \frac{-aT}{C_{\rm capacity}} \\ \frac{T}{C_{\rm fast}} \\ \frac{T}{C_{\rm slow}} \end{bmatrix} I_{\rm batt}(k), \tag{3}$$

where the battery terminal voltage $U_{\rm batt}$ is given with

$$U_{\rm batt}(k) = V_{\rm OC}(k) - V_{\rm fast}(k) - V_{\rm slow}(k) - R_{\rm serial} I_{\rm batt}(k), \tag{4}$$

where $V_{\rm fast}$ is the voltage at the fast-transient RC network, $V_{\rm slow}$ is the voltage at the slow-transient RC network. Notion $z(k)$ denotes the value of any variable z at the discrete-time instant kT, $k \in \mathbb{Z}$, while the battery state is denoted with $x = [V_{\rm OC}, V_{\rm fast}, V_{\rm slow}]^T$. According to Fig. 2, charging currents are negative, while discharging currents are positive.

B. Energy for battery charging and discharging

The energy that needs to be exchanged between the battery and the microgrid in time NT can be expressed with (power converter losses are neglected)

$$E = \int_0^{NT} U_{\rm batt}(t) I_{\rm batt}(t) {\rm d}t. \tag{5}$$

After calculation of the energy using the hybrid electrical model with assuming the battery current is constant between the discrete-time sampling instants, the following expression of energy for battery charging and discharging is obtained:

$$E = {\mathbf{I}_{\rm batt}}^T H \mathbf{I}_{\rm batt} + x(0)^T F_1^T \mathbf{I}_{\rm batt}, \tag{6}$$

where $\mathbf{I}_{\rm batt}$ is $N \times 1$ vector which contains the current values with the sampling time T from k=0 to k=$N-1$, H is $N \times N$ symmetric negative definite matrix and F_1 is $N \times 3$ matrix.

III. Open-loop optimization problem

In the sequel the open-loop optimization problem for efficient adherence to an energy exchange command under longevity constraints is defined and all steps for its solving with the corresponding algorithms are presented.

A. Problem formulation

The BMS receives from the microgrid energy flows optimization level the control commands on energies that need to be exchanged between the battery and the microgrid in the given time. In order to get the battery current profile for adherence to the issued energy exchange command that respects the given longevity constraints and maximizes efficiency by maximizing the residual battery SOC, the following optimization problem for battery charging and discharging is posed:

$$\begin{aligned} &\max_{\mathbf{I}_{\rm batt}} SOC(N) = SOC(0) + C_{\rm m}^T \mathbf{I}_{\rm batt} \\ &\text{s.t.} \quad {\mathbf{I}_{\rm batt}}^T H \mathbf{I}_{\rm batt} + x(0)^T F_1^T \mathbf{I}_{\rm batt} = E_{\rm com}, \\ &I_{\rm batt-d} \geq I_{\rm batt}(k) \geq -I_{\rm batt-c}, \quad k = 0, \ldots, N-1, \\ &U_{\rm battmin} \leq U_{\rm batt}(k) \leq U_{\rm battmax}, \quad k = 0, \ldots, N-1, \\ &U_{\rm battmin} \leq U^-_{\rm batt}(k) \leq U_{\rm battmax}, \quad k = 1, \ldots, N, \\ &SOC_{\rm battmin} \leq SOC(k) \leq SOC_{\rm battmax}, \quad k = 1, \ldots, N, \end{aligned} \tag{7}$$

where $E_{\rm com}$ is the commanded energy that needs to be exchanged between the battery and the microgrid in the fixed amount of time NT, $I_{\rm batt-d}$ is the maximal discharging

current, $I_{\mathrm{batt-c}}$ is the maximal absolute value of the charging current, U_{battmin} is the lower voltage limit and U_{battmax} is the upper voltage limit of the battery. SOC_{battmin} and SOC_{battmax} are the upper and lower SOC limits, respectively. $U^{-}_{\mathrm{batt}}(k)$ as the battery voltage just before the new current at time kT is applied is also introduced such that the battery voltage does not exceed the limits even between the discrete-time sampling instants:

$$U^{-}_{\mathrm{batt}}(k) = \lim_{t \to kT^{-}} U_{\mathrm{batt}}(t) = V_{\mathrm{OC}}(k) - V_{\mathrm{fast}}(k) - V_{\mathrm{slow}}(k) - R_{\mathrm{serial}} I_{\mathrm{batt}}(k-1).$$

Vector C_{m} in the cost function of (7) is

$$C_{\mathrm{m}} = \begin{bmatrix} -T/C_{\mathrm{capacity}} & \dots & -T/C_{\mathrm{capacity}} \end{bmatrix}. \tag{8}$$

The constraints for ensuring longevity of a battery are defined with inequalities of the optimization problem (7) and the numerical values for these limits can be found in the battery manufacturer datasheet or derived from it.

The first two inequalities in (7) define the constraints for the maximal charging and the maximal discharging current. VRLA batteries are significantly sensitive to high charging currents due to their exposure to an increased secondary electrochemical reactions in such a situation (the oxygen generation and the grid corrosion on the positive electrode, the hydrogen generation on the negative electrode), which cause an increase of the degradation effects within the battery cells [32], and a premature loss of the battery capacity. The high discharging currents are not damaging as high charging currents and their maximum values provided by the manufacturers are significantly higher compared to the charging currents (e.g., $I_{\mathrm{batt-d}} \cong 12 I_{\mathrm{batt-c}}$).

VRLA batteries are also sensitive to too high voltage which causes an increase of the degradation effects during charging [33], [34]. Too low voltage at battery electrodes is damaging due to higher sulphation on the negative electrode which leads to the loss of capacity [8]. In order to protect the battery from too high and too low voltages, the next four inequalities are defined in the optimization problem (7).

The maximal and minimal SOC constraints are defined with the last two inequalities in (7). These constraints are useful in order to prevent the battery from underdischarging which causes higher sulphation on the negative electrode and from overcharging which causes the increased secondary electrochemical reactions.

The batteries which violate these constraints during charging/discharging are exposed to the aforementioned reactions in battery cells. Therefore, these constraints must be respected such that the battery can have its lifetime as declared by the manufacturer.

B. Unconstrained optimal battery charging/discharging under commanded energy flow

In case of absence of all the inequality constraints in (7), the resulting optimization problem can be solved by using the method of Lagrange multipliers which involves the modification of the objective function through the addition of terms that describe the equality constraints [35], [36]. The augmented objective function is called Lagrange function and for the optimization problem with equality constraint it is as follows:

$$\mathcal{L} = SOC(N) + \lambda(\mathbf{I}_{\mathrm{batt}}{}^{T} H \mathbf{I}_{\mathrm{batt}} + x(0)^{T} F_1^{T} \mathbf{I}_{\mathrm{batt}} - E_{\mathrm{com}}), \tag{9}$$

where $\lambda \in \mathbb{R}$ is the Lagrange multiplier.

In order to maximize the Lagrange function (9), the partial derivatives with respect to control variables $\mathbf{I}_{\mathrm{batt}}$ and to λ are taken and $N+1$ equations with $N+1$ unknowns are obtained:

$$C_{\mathrm{m}}^{T} + 2\lambda H \mathbf{I}_{\mathrm{batt}} + \lambda F_1 x(0) = 0, \tag{10}$$

$$\mathbf{I}_{\mathrm{batt}}{}^{T} H \mathbf{I}_{\mathrm{batt}} + x(0)^{T} F_1^{T} \mathbf{I}_{\mathrm{batt}} - E_{\mathrm{com}} = 0. \tag{11}$$

The solution of $\mathbf{I}_{\mathrm{batt}}$ from the previous equations is

$$\mathbf{I}_{\mathrm{batt}} = H^{-1} \cdot \frac{-F_1 x(0)\lambda - C_{\mathrm{m}}}{2\lambda}, \tag{12}$$

and λ that maximizes (9) is

$$\lambda = +\sqrt{\frac{C_{\mathrm{m}}^{T} H^{-1} C_{\mathrm{m}}}{x(0)^{T} F_1^{T} H^{-1} F_1 x(0) + 4E_{\mathrm{com}}}}. \tag{13}$$

C. Recursive feasibility of the optimization problem

Invariant set is an important tool in control of dynamical systems due to its ability to enable the designer to guarantee that state trajectories starting inside it will remain inside forever by employing suitable admissible control actions [37]–[39].

Definition 4.1. Controlled invariant set. For the system $x(k+1) = f(x(k), u(k)), x \in \mathbb{R}^n, u \in \mathbb{R}^m$ and constraints defining set $C^{\mathrm{xu}} \subseteq \mathbb{R}^{\mathrm{n+m}}$, a set $\mathcal{S} \subseteq \underset{\mathbb{R}^n}{\mathrm{proj}}\, C^{\mathrm{xu}}$ (with $\underset{\mathbb{R}^n}{\mathrm{proj}}$ we denote the operator of set projection onto the first n dimensions of the space in which the set lies) is controlled invariant if for all $x \in \mathcal{S}$ there exists an admissible control action u that retains the state in $\mathcal{S}$, i.e.:

$$\begin{bmatrix} x \\ u \end{bmatrix} \in C^{\mathrm{xu}},$$
$$f(x,u) \in \mathcal{S}.$$

In case of linearly constrained linear systems the controlled invariant set is polyhedral and can be thus presented using the following expression [40]:

$$\mathcal{S} = \{x \in \mathbb{R}^n \mid P^{\mathrm{x}} x \ \leq \ P^{\mathrm{c}}\}, \tag{14}$$

where inequality $P^{\mathrm{x}} x \ \leq \ P^{\mathrm{c}}$, with $P^{\mathrm{x}} \in \mathbb{R}^{h \times n}$, $P^{\mathrm{c}} \in \mathbb{R}^{h}$, is considered component-wise, while h is the number of halfspaces defining the polytope $\mathcal{S}$ with their intersection.

In order to ensure recursive feasibility of the control problem (7) with inequality constraints the state at the end of the prediction horizon $x(N)$ of the battery state sequence has to be inside the controlled invariant set $\mathcal{S}$. Thus, besides the aforementioned constraints in (7), additional constraint is used in the optimization problem to ensure its recursive feasibility, as follows:

$$P^{\mathrm{x}} x(N) \leq P^{\mathrm{c}}, \tag{15}$$

and the optimization problem (7) can be enlarged to the following form:

$$\begin{aligned}
&\max_{\mathbf{I}_{\mathrm{batt}}} SOC(N) = SOC(0) + C_{\mathrm{m}}^T \mathbf{I}_{\mathrm{batt}} \\
&\text{s.t.} \quad {\mathbf{I}_{\mathrm{batt}}}^T H \mathbf{I}_{\mathrm{batt}} + x(0)^T F_1^T \mathbf{I}_{\mathrm{batt}} = E_{\mathrm{com}}, \\
&I_{\mathrm{batt-d}} \geq I_{\mathrm{batt}}(k) \geq -I_{\mathrm{batt-c}}, \quad k = 0, \ldots, N-1, \\
&U_{\mathrm{battmin}} \leq U_{\mathrm{batt}}(k) \leq U_{\mathrm{battmax}}, \quad k = 0, \ldots, N-1, \\
&U_{\mathrm{battmin}} \leq U_{\mathrm{batt}}^-(k) \leq U_{\mathrm{battmax}}, \quad k = 1, \ldots, N, \\
&SOC_{\mathrm{battmin}} \leq SOC(k) \leq SOC_{\mathrm{battmax}}, \quad k = 1, \ldots, N, \\
&P^x x(N) \leq P^c.
\end{aligned} \tag{16}$$

Inequality constraints in (16) can be presented as constraints on the battery current sequence $\mathbf{I}_{\mathrm{batt}}$ and the initial state $x(0)$ which finally yields the set $\mathcal{S}_{\mathrm{I}}$ of admissible current sequences:

$$P_{\mathrm{I}} \mathbf{I}_{\mathrm{batt}} \leq P_{\mathrm{c}} + P_{\mathrm{x}} x(0). \tag{17}$$

D. Determination of the minimal and the maximal energy manageable with the Lagrange multipliers method in the presence of battery constraints

The battery current (12) is a function of initial battery state $x(0)$ and Lagrange multiplier λ. In order to simplify the analysis, the new variable $\kappa = 1/\lambda$ is introduced and the expression (12) can be written in the following form:

$$\mathbf{I}_{\mathrm{batt}} = -\frac{1}{2} H^{-1} F_1 x(0) - \frac{1}{2} H^{-1} C_{\mathrm{m}} \kappa. \tag{18}$$

Introducing (18) in (17), the following expression is obtained in $(n+1)$-dimensional polytope form:

$$\begin{bmatrix} P_{\mathrm{x1}} & P_\kappa \end{bmatrix} \begin{bmatrix} x(0) \\ \kappa \end{bmatrix} \leq \begin{bmatrix} P_{\mathrm{c}} \end{bmatrix}, \tag{19}$$

and the set described in (19) is denoted with $\mathcal{S}_{\mathrm{x}-\kappa}$. By applying the projection of the polytope $\mathcal{S}_{\mathrm{x}-\kappa}$ on the battery state space, the polytope $\mathcal{S}_{\mathrm{proj}}$ is obtained to which it applies $\mathcal{S}_{\mathrm{proj}} \in \mathcal{S}$, and it is denoted with

$$P_{\mathrm{x-proj}} x(0) \leq P_{\mathrm{c-proj}}. \tag{20}$$

For each initial state $x(0)$ inside the polytope $\mathcal{S}_{\mathrm{proj}}$, there exist energies that can be exchanged between the battery and the microgrid in the prescribed timeframe NT such that the currents for this exchange can be obtained by using the method of Lagrange multipliers. The solution of the unconstrained optimization problem for adherence to the energy exchange command via Lagrange multipliers is for such commanded energy exchanges and states also optimal in the presence of constraints for the full optimization problem (16) as it by the above construction satisfies all these constraints. For other initial states which are not inside the polytope $\mathcal{S}_{\mathrm{proj}}$, while belonging to the invariant set $\mathcal{S}$, there are no solutions using the method of Lagrange multipliers for any energy exchange command.

If the initial state $x(0)$ belongs to the polytope $\mathcal{S}_{\mathrm{proj}}$, the minimal energy E_{minLG} and the maximal energy E_{maxLG}, that can be exchanged between the battery and the microgrid without violating the aforementioned battery constraints, can be calculated using the method of Lagrange multipliers. Before calculations of battery current and energy, firstly it is necessary to determine the maximal and the minimal values of variable κ. Using the expression (19) for fixed $x(0)$ a convex interval $\mathcal{K}(x(0))$ of admissible values of κ is calculated.

After determination of the interval $\mathcal{K}(x(0))$, it is necessary to determine its extremes, i.e. the minimal value $\kappa_{\min} = \min_{\kappa \in \mathcal{K}(x(0))} \kappa$ and the maximal value $\kappa_{\max} = \max_{\kappa \in \mathcal{K}(x(0))} \kappa$. Using the expression (18), the obtained extreme values of κ are used for calculation of the corresponding current sequences $\mathbf{I}_{\mathrm{minLG}}$ and $\mathbf{I}_{\mathrm{maxLG}}$. If $0 \in \mathcal{K}(x(0))$, $\mathbf{I}_{\mathrm{maxLG}}$ corresponds to $\kappa = 0$. Finally, the minimal energy E_{minLG} and the maximal energy E_{maxLG} are calculated using the expression (6) with the corresponding current sequences ($\mathbf{I}_{\mathrm{minLG}}$, $\mathbf{I}_{\mathrm{maxLG}}$) for the given initial state $x(0)$.

E. The minimal and maximal attainable energy in the presence of all operational battery constraints

The battery constraints (17) expressed with respect to the control variable $\mathbf{I}_{\mathrm{batt}}$ present an N-dimensional polytope $\mathcal{S}_{\mathrm{I}}$ for a fixed $x(0)$.

The maximal energy that can be exchanged between the battery and the microgrid can be calculated using a Quadratic Program (QP) with the objective function (6) for a given initial state $x(0)$ inside the controlled invariant set $\mathcal{S}$:

$$\begin{aligned}
\max_{\mathbf{I}_{\mathrm{batt}}} \quad & {\mathbf{I}_{\mathrm{batt}}}^T H \mathbf{I}_{\mathrm{batt}} + x(0)^T F_1^T \mathbf{I}_{\mathrm{batt}} \\
\text{s.t.} \quad & P_{\mathrm{I}} \mathbf{I}_{\mathrm{batt}} \leq P_{\mathrm{c}} + P_{\mathrm{x}} x(0).
\end{aligned} \tag{21}$$

The minimal energy of the battery for a given initial state $x(0)$ inside the controlled invariant set $\mathcal{S}$ cannot be calculated using a QP due to the negative definiteness of matrix H. For minimization of energy a non-convex problem is obtained using the expression (6):

$$\begin{aligned}
\min_{\mathbf{I}_{\mathrm{batt}}} \quad & {\mathbf{I}_{\mathrm{batt}}}^T H \mathbf{I}_{\mathrm{batt}} + x(0)^T F_1^T \mathbf{I}_{\mathrm{batt}} \\
\text{s.t.} \quad & P_{\mathrm{I}} \mathbf{I}_{\mathrm{batt}} \leq P_{\mathrm{c}} + P_{\mathrm{x}} x(0).
\end{aligned} \tag{22}$$

Here an iterative solving algorithm can be employed but it does not always guarantee attaining the global minimum. The Sequential Linear Program (SLP) is an iterative method that generates and solves a sequence of linear problems until achieving the convergence to a solution. Primarily, the Chebyshev center of $\mathcal{S}_{\mathrm{I}}$ is calculated and initial current sequence $\mathbf{I}_{\mathrm{batt}}(0) := \mathbf{I}_{\mathrm{CH}}$ for SLP is obtained. After that, expression (6) has to be linearized with respect to the current, and in that form is used as the objective function in an iterative Linear Program (LP) as follows:

$$\begin{aligned}
\mathbf{I}_{\mathrm{batt}}(i+1) = \arg\min_{\mathbf{I}_{\mathrm{batt}}} \quad & (2\mathbf{I}_{\mathrm{batt}}(i)^T H + x(0)^T F_1^T) \mathbf{I}_{\mathrm{batt}} \\
\text{s.t.} \quad & P_{\mathrm{I}} \mathbf{I}_{\mathrm{batt}} \leq P_{\mathrm{c}} + P_{\mathrm{x}} x(0).
\end{aligned} \tag{23}$$

The iterative procedure using LP is repeated until the solution is equal in two consecutive iterations. With $\mathbf{I}_{\mathrm{SLP}}$ is denoted the solution of the SLP algorithm (23). The attainable energy E_{minSLP} can be calculated using the expression (6) and the obtained $\mathbf{I}_{\mathrm{SLP}}$ for a given initial state $x(0)$.

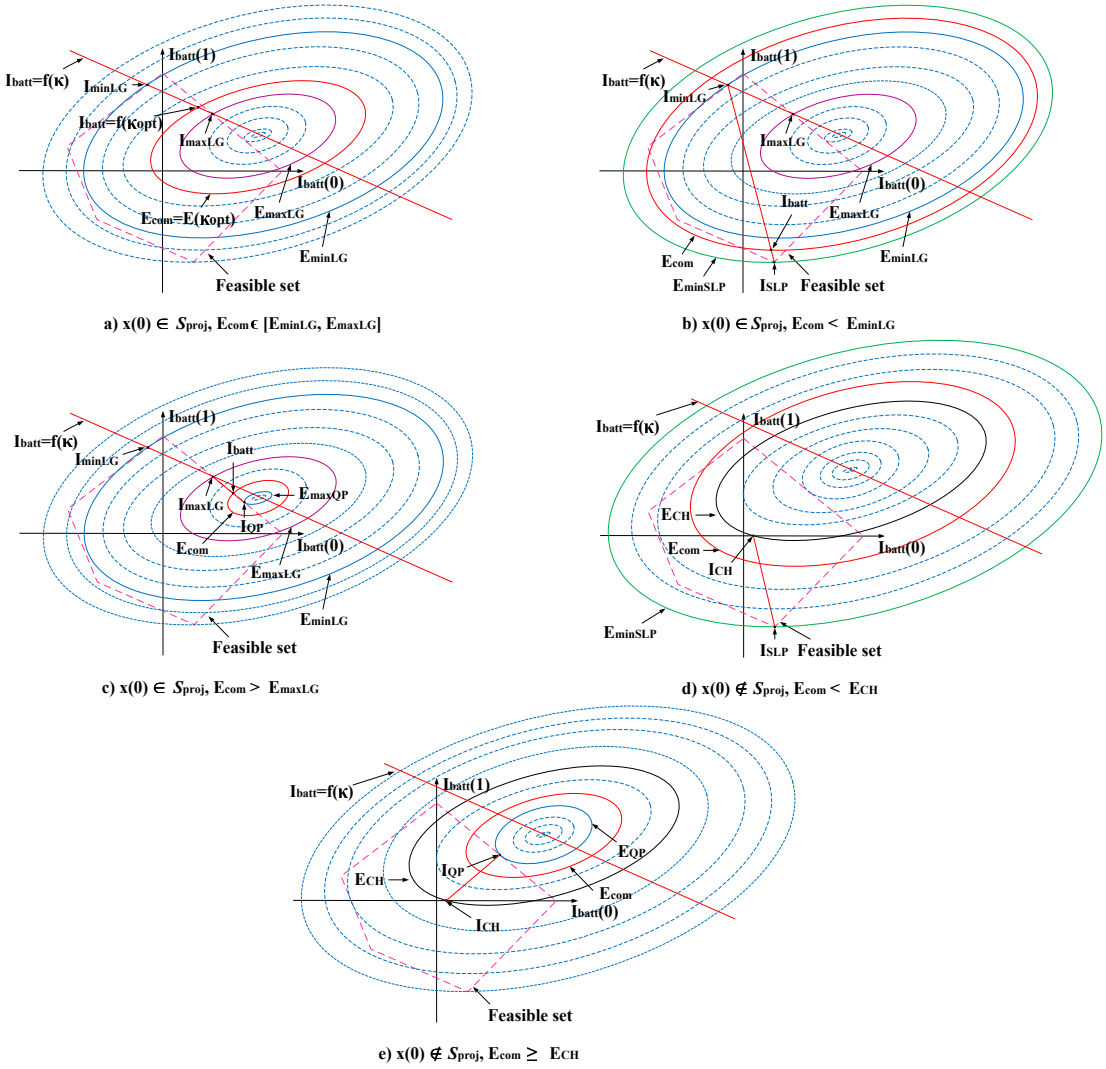

Fig. 3. Value levels of the energy function in the space of battery currents through the prediction horizon for a fixed battery initial state (for simplicity of the illustration, it was presumed that N = 2, i.e. that there are only two currents for prediction along the prediction horizon: $I_{\mathrm{batt}}(0)$ and $I_{\mathrm{batt}}(1)$). Feasible set from (17) is also depicted, as well as the line which illustrates the relation between κ and the predicted currents profile determined with (18). The five possible cases depending on the initial state and the commanded energy flow are shown.

F. Algorithm for control of the battery charging and discharging for adherence to the commanded energy flow

In this section the algorithm for solving the problem (16) and ensuring its recursive feasibility is completely shown.

If the initial state $x(0)$ of the invariant set $\mathcal{S}$ is inside the polytope $\mathcal{S}_{\mathrm{proj}}$ and $E_{\mathrm{com}} \in [E_{\mathrm{minLG}}, E_{\mathrm{maxLG}}]$, the current sequence $\mathbf{I}_{\mathrm{batt}}$ is calculated using the method of Lagrange multipliers. This case is shown in Fig. 3.a). For $x(0) \in \mathcal{S}_{\mathrm{proj}}$, in cases of $E_{\mathrm{com}} < E_{\mathrm{minLG}}$ (Fig. 3.b)) or $E_{\mathrm{com}} > E_{\mathrm{maxLG}}$ (Fig. 3.c)), SLP or QP are applied to calculate the current sequences $\mathbf{I}_{\mathrm{SLP}}$ or $\mathbf{I}_{\mathrm{QP}}$, respectively. The initial battery currents for the consequent iterative solving procedure in both cases are obtained as convex combinations of ($\mathbf{I}_{\mathrm{SLP}}$, $\mathbf{I}_{\mathrm{minLG}}$) or ($\mathbf{I}_{\mathrm{maxLG}}$, $\mathbf{I}_{\mathrm{QP}}$), respectively, to ensure reaching the ellipsoid determined by (6). The convex combination can be used because the energy exchange with the battery is a continuous (quadratic) function of the applied current profile. Thus the connection between any two current profiles contains currents that result in all energies between the energies for these two bordering profiles, as shown in Fig. 3. After the initial current is determined that respects all constraints and satisfies the equality criterion for the energy flow, we continue to search the solution to (16) by iteratively sliding along the ellipsoid of the commanded energy exchange in the direction of maximization of $SOC(N)$.

For each initial state $x(0)$ of the invariant set $\mathcal{S}$ which is not inside the polytope $\mathcal{S}_{\mathrm{proj}}$, no points in the polytope $\mathcal{S}_{\mathrm{I}}$ can be determined via the Lagrange multipliers method since there is no feasible Lagrange multiplier for any required energy flow. In that case, firstly the current sequence $\mathbf{I}_{\mathrm{CH}}$ as Chebyshev center of polytope $\mathcal{S}_{\mathrm{I}}$ and the respective energy E_{CH} are calculated. E_{CH} is then compared to the commanded energy E_{com}. In cases of $E_{\mathrm{com}} < E_{\mathrm{CH}}$ (Fig. 3.d)) or $E_{\mathrm{com}} \geq E_{\mathrm{CH}}$ (Fig. 3.e)), SLP or QP are applied to calculate the current sequences $\mathbf{I}_{\mathrm{SLP}}$ or $\mathbf{I}_{\mathrm{QP}}$, respectively. The initial battery currents for both cases are obtained as convex combinations of ($\mathbf{I}_{\mathrm{SLP}}$, $\mathbf{I}_{\mathrm{CH}}$) or ($\mathbf{I}_{\mathrm{CH}}$, $\mathbf{I}_{\mathrm{QP}}$), respectively, to reach the ellipsoid defined by

Algorithm 1 Algorithm for prediction of the battery current for attaining the required energy flow and maximizing $SOC(N)$ under longevity and recursive feasibility constraints

$x(0) \in \mathcal{S}$, E_{com} ▷ *Initial state, commanded energy*
if $x(0) \in \mathcal{S}_{\mathrm{proj}}$ **then**
  Calculate $\mathcal{K}(x(0))$ ▷ *Method of Lagrange multipliers*
  $\kappa_{\min} = \min_{\kappa \in \mathcal{K}(x(0))} \kappa$; $\kappa_{\max} = \max_{\kappa \in \mathcal{K}(x(0))} \kappa$
  Calculate $\mathbf{I}_{\mathrm{minLG}}$, E_{minLG} and $\mathbf{I}_{\mathrm{maxLG}}$, E_{maxLG}
  if $E_{\mathrm{com}} \in [E_{\mathrm{minLG}}, E_{\mathrm{maxLG}}]$ **then**
    Calculate $\mathbf{I}_{\mathrm{batt}}$ using the method of Lagrange multipliers
  else if $E_{\mathrm{com}} < E_{\mathrm{minLG}}$ **then**
    Calculate $\mathbf{I}_{\mathrm{SLP}}$, E_{minSLP} ▷ *Applying SLP*
    Calculate α in $\mathbf{I}_{\mathrm{batt}} = \alpha \mathbf{I}_{\mathrm{SLP}} + (1-\alpha)\mathbf{I}_{\mathrm{minLG}}$, $\alpha \in [0,1]$ such that $E(\mathbf{I}_{\mathrm{batt}}) = E_{\mathrm{com}}$
    $\mathbf{I}_{\mathrm{batt}}$ = iteratively slide towards the optimum $(\mathbf{I}_{\mathrm{batt}}, \mathbf{I}_{\mathrm{minLG}}, H, F_1, x(0), P_{\mathrm{I}}, P_{\mathrm{c}}, P_{\mathrm{x}}, C_{\mathrm{m}})$
  else
    Calculate $\mathbf{I}_{\mathrm{QP}}$, E_{maxQP} ▷ *Applying QP*
    Calculate α in $\mathbf{I}_{\mathrm{batt}} = \alpha \mathbf{I}_{\mathrm{maxLG}} + (1-\alpha)\mathbf{I}_{\mathrm{QP}}$, $\alpha \in [0,1]$ such that $E(\mathbf{I}_{\mathrm{batt}}) = E_{\mathrm{com}}$
    $\mathbf{I}_{\mathrm{batt}}$ = iteratively slide towards the optimum $(\mathbf{I}_{\mathrm{batt}}, \mathbf{I}_{\mathrm{maxLG}}, H, F_1, x(0), P_{\mathrm{I}}, P_{\mathrm{c}}, P_{\mathrm{x}}, C_{\mathrm{m}})$
  end if
else if $x(0) \notin \mathcal{S}_{\mathrm{proj}}$ **then**
  Calculate $\mathbf{I}_{\mathrm{CH}}$ ▷ *Calculation of Chebyshev center of* $\mathcal{S}_{\mathrm{I}}$
  Calculate E_{CH}
  if $E_{\mathrm{com}} < E_{\mathrm{CH}}$ **then**
    Calculate $\mathbf{I}_{\mathrm{SLP}}$, E_{minSLP} ▷ *Applying SLP*
    Calculate α in $\mathbf{I}_{\mathrm{batt}} = \alpha \mathbf{I}_{\mathrm{SLP}} + (1-\alpha)\mathbf{I}_{\mathrm{CH}}$, $\alpha \in [0,1]$ such that $E(\mathbf{I}_{\mathrm{batt}}) = E_{\mathrm{com}}$
    $\mathbf{I}_{\mathrm{batt}}$ = iteratively slide towards the optimum $(\mathbf{I}_{\mathrm{batt}}, \mathbf{I}_{\mathrm{CH}}, H, F_1, x(0), P_{\mathrm{I}}, P_{\mathrm{c}}, P_{\mathrm{x}}, C_{\mathrm{m}})$
  else
    Calculate $\mathbf{I}_{\mathrm{QP}}$, E_{maxQP} ▷ *Applying QP*
    Calculate α in $\mathbf{I}_{\mathrm{batt}} = \alpha \mathbf{I}_{\mathrm{CH}} + (1-\alpha)\mathbf{I}_{\mathrm{QP}}$, $\alpha \in [0,1]$ such that $E(\mathbf{I}_{\mathrm{batt}}) = E_{\mathrm{com}}$
    $\mathbf{I}_{\mathrm{batt}}$ = iteratively slide towards the optimum $(\mathbf{I}_{\mathrm{batt}}, \mathbf{I}_{\mathrm{CH}}, H, F_1, x(0), P_{\mathrm{I}}, P_{\mathrm{c}}, P_{\mathrm{x}}, C_{\mathrm{m}})$
  end if
end if

the equality constraint (6). After that, analogously as for the two cases from above, iterative sliding along the ellipsoid of the commanded energy in the direction of maximization of $SOC(N)$ takes place.

In the sequel all steps of the overall algorithm are presented: Algorithm 1, as well as the steps of the iterative sliding along the ellipsoid of the commanded energy flow under constraints in the direction of maximization of $SOC(N)$ (Algorithm 2). In Algorithm 2 the value 10^{-6} is used as a numerical tolerance of the algorithm. We assume all hyperplanes are defined with their normal vectors already normalized.

IV. Closed-loop control algorithm

In the sequel the closed-loop control for battery charging and discharging with adherence to energy flow commands from the level of microgrid energy flows optimization is introduced.

At each sampling instant the BMS replans the battery current profile on the remaining timeframe part using the open-loop optimization problem (16). Accordingly, the commanded energy exchange is precisely adhered to while respecting battery constraints and maximizing the residual state of charge. The closed-loop control enables to perform the exactly required energy exchange in the presence of various disturbances and the battery model inaccuracies [41].

If j is the absolute discrete time for any time $t = jT$, then the time step i is defined with expression $i = j \mathrm{mod}(\mathrm{T}_{\mathrm{MGR}}/\mathrm{T})$ where T_{MGR} is the sampling time of microgrid energy flow optimization. Furthermore, $E_{\mathrm{com}}^{\mathrm{mgr}}$ is the overall commanded energy exchange between the battery and the microgrid within T_{MGR}, while $E_{\mathrm{ach}}(i)$ is the achieved energy calculated as a numerical integral of the battery power profile in the time interval corresponding to time indices from 0 to i.

Closed-loop control algorithm for adherence to the energy flow command is provided as follows:

$$\begin{gathered} N = T_{\mathrm{MGR}}/T - i, \\ E_{\mathrm{com}} = E_{\mathrm{com}}^{\mathrm{mgr}} - E_{\mathrm{ach}}(i), \\ x(0) = x(i), \\ \text{Solve (16)}, \\ \text{Implement } \mathbf{I}_{\mathrm{batt}}(0) \text{ to the battery power converter.} \end{gathered} \tag{24}$$

V. Simulation and experimental results

For simulations and experiments a 48 V VRLA battery with 45 Ah nominal capacity is used [42]. The open-loop and closed-loop control algorithms are implemented in Matlab using the mathematical programming solver CPLEX [43].

Algorithm 2 Iterative sliding along the ellipsoid of the commanded energy flow in the direction of maximization of the $SOC(N)$

$\mathbf{I}_{\mathrm{batt}}$, $\mathbf{I}_{\mathrm{n}}$, $x(0) \in \mathcal{S}$, H, F_1, P_{I}, P_{c}, P_{x}, C_{m} ▷ $\mathbf{I}_{\mathrm{n}}$ – *reference current sequence*
Use $x(0)$ to calculate matrices A_1 and vector b_1 of the polytope $\mathcal{S}_{\mathrm{I}}$ description
$c_{\mathrm{m}} = C_{\mathrm{m}}/\mathrm{norm}(C_{\mathrm{m}})$
step = 1
base = [ ]
$m = 0$
$\mathbf{I}_{\mathrm{batt}}(0) = \mathbf{I}_{\mathrm{batt}}$
while number of rows in base $\leq$ dim($\mathbf{I}_{\mathrm{batt}}$) **do**
    max-row = max($A_1\mathbf{I}_{\mathrm{batt}}(m) - b_1$)
    while max-row $\leq 10^{-6}$ **do**
        $c = 2H\mathbf{I}_{\mathrm{batt}}(m) + F_1x(0)$ ▷ *Vector of the ellipsoid tangent plane*
        W = null([c^T; base]) ▷ *Base of the allowed space for current change*
        if norm(W^Tc_{m}) $\leq 10^{-6}$ **then**
            finish = 1
            break
        end if
        $v = W(W^Tc_{\mathrm{m}})$ ▷ *Direction of improvement of the solution in the tangent plane*
        $v_{\mathrm{n}} = v/\mathrm{norm}(v)$
        while $\mathbf{I}_{\mathrm{batt}}(m) \in \mathcal{S}_{\mathrm{I}}$ **do**
            $\mathbf{I}_{\mathrm{tang}} = \mathbf{I}_{\mathrm{batt}}(m)$+ step v_{n} ▷ *The current shift in the tangent plane*
            Calculate α in $\mathbf{I}_{\mathrm{batt}}(m+1) = \alpha\mathbf{I}_{\mathrm{tang}} + (1-\alpha)\mathbf{I}_{\mathrm{n}}$, $\alpha \in [0,1]$ such that $E(\mathbf{I}_{\mathrm{batt}}) = E_{\mathrm{com}}$
            if $\mathbf{I}_{\mathrm{batt}}(m+1) \notin \mathcal{S}_{\mathrm{I}}$ **then**
                step = step/2
            end if
            max-row = max($A_1\mathbf{I}_{\mathrm{batt}}(m+1) - b_1$)
            $m := m + 1$
        end while
    end while
    if max-row $\geq 10^{-6}$ **then**
        $\mathbf{I}_{\mathrm{n}}$ = $\mathbf{I}_{\mathrm{batt}}(m+1)$
        ind = find($(A_1\mathbf{I}_{\mathrm{batt}}(m+1) - b_1) \geq -10^{-6}$)
        base = [base; A_1(ind, :)] ▷ *Allow further changes of current only along activated constraints*
        Remove from A_1 and b_1 all rows with indices from ind
    end if
    if finish = 1 **then**
        break
    end if
end while
$\mathbf{I}_{\mathrm{batt}} = \mathbf{I}_{\mathrm{batt}}$(end)

Sampling times $T = 1$ min and $T_{\mathrm{MGR}} = 60$ min are chosen. The battery model parameters (R_{serial}, R_{fast}, R_{slow}, C_{fast}, and C_{slow}) are determined from the corresponding voltage-time curves which are obtained using a method with resting periods during the experimental charging and discharging. More on the parameter identification procedure can be found in [28], [44] and the obtained values of the battery parameters are shown in Table I. To validate the parameters of the hybrid electrical model a comparison between the experimental data and simulations obtained by the model during the pulse charging and discharging with the current 17.2 A is performed. This validation for charging and discharging is shown in Fig. 4 and one can see that there are slight discrepancies between the model and measured data which are visible at high and low levels of SOC but still the application of (1) considering the use of closed-loop Model Predictive Control (MPC) for model inaccuracies alleviation is justified.

The numerical values of all additional constraints of the considered VRLA battery stack are shown in Table II and they are defined using the manufacturer data-sheet [42]. Accordingly, recommended operating window of 100% for depth of discharge in [42] is also taken into account. This operating window defines numerical values for lower and upper SOC limits in Table II. The selection of SOC limits can of course be different in other applications.

A. Open-loop control analysis

By using the values for longevity constraints defined in Table II, the controlled invariant set $\mathcal{S}$ for this battery stack is

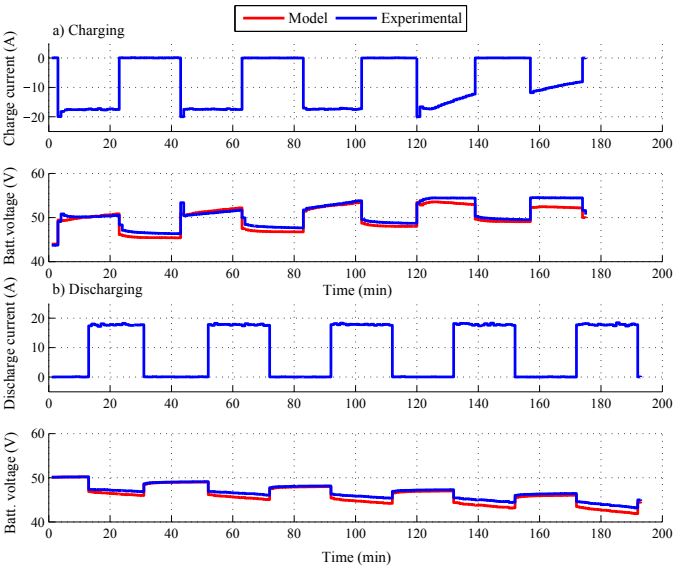

Fig. 4. Validation of the hybrid electrical model during the pulse charging and discharging with the current 17.20 A

TABLE I
THE HYBRID ELECTRICAL MODEL PARAMETERS

Symbol	Description	Value
R_{serial}	Serial resistance	0.1395 Ω
R_{fast}	Fast-transient resistance	0.0806 Ω
R_{slow}	Slow-transient resistance	0.0465 Ω
C_{capacity}	Battery capacitance	129600 F
C_{fast}	Fast-transient capacitance	3400 F
C_{slow}	Slow-transient capacitance	89145 F
a	Open-circuit voltage parameter	7.70 V
b	Open-circuit voltage parameter	44.20 V

TABLE II
NUMERICAL VALUES FOR THE BATTERY LONGEVITY CONSTRAINTS

Symbol	Description	Value
$I_{\text{batt}-\text{c}}$	Maximal charging current	17.20 A
U_{battmax}	Upper voltage limit	54.50 V
SOC_{battmax}	Upper SOC limit	100 %
$I_{\text{batt}-\text{d}}$	Maximal discharging current	206.40 A
U_{battmin}	Lower voltage limit	42.00 V
SOC_{battmin}	Lower SOC limit	0 %

calculated with the help of Multi-Patrametric Toolbox (MPT) [45]. The obtained invariant set $\mathcal{S}$, shown in Fig. 5, has 450 hyperplanes. Additionally, the polytope $\mathcal{S}_{\text{x}-\kappa}$ (19) can be calculated for all prediction horizons N = 1,...,60.

In the sequel, analyses of five different cases in dependence of the initial state $x(0)$ and the commanded energy E_{com} that needs to be exchanged between the battery and the microgrid (see Fig. 3), are presented.

a) Case 1 ($x(0) \in \mathcal{S}_{\text{proj}}$, $E_{\text{com}} \in [E_{\text{minLG}}, E_{\text{maxLG}}]$): The initial state $x(0)$ is inside the polytope $\mathcal{S}_{\text{proj}}$, while commanded energy E_{com} is 500 Wh. The current sequence is positive during the whole hour and the battery stack is discharging. All current values are significantly less than the

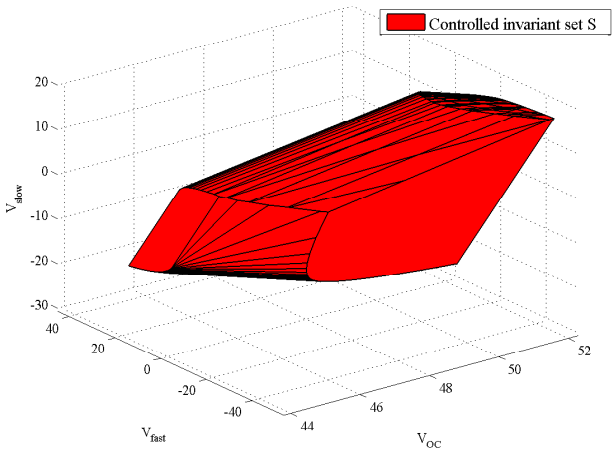

Fig. 5. The polyhedral controlled invariant set $\mathcal{S}$ of states for the VRLA battery considered

maximal discharging current ($I_{\text{batt}} \leq 206.40$ A), as shown in Fig. 6. Also, the states of the battery stack and their changes along the prediction horizon are presented in this figure. In order to show all states in the same range, open-circuit voltage V_{OC} is presented as difference $V_{\text{OC}} - V_{\text{min}}$, where V_{min} = 44.20 V. Further, it can be seen that all voltage and SOC values are within their allowed constraints.

b) Case 2 ($x(0) \in \mathcal{S}_{\text{proj}}$, $E_{\text{com}} < E_{\text{minLG}}$): The initial state $x(0)$ is inside the polytope $\mathcal{S}_{\text{proj}}$, while commanded energy E_{com} is -450 Wh. The initial battery current is calculated as convex combination of $\mathbf{I}_{\text{SLP}}$ and $\mathbf{I}_{\text{minLG}}$ and then iterative sliding along the ellipsoid towards the maximum of $SOC(N)$ is performed to finally obtain the optimal current profile. In this case the battery stack is charging due to negative values of the current sequence during the simulation, as shown in Fig. 7. The algorithm keeps the current of the battery stack below the maximal charging current (17.20 A) provided by the manufacturer. Also, the battery SOC is not close to the upper and lower limit. Furthermore, the battery voltage is very close to the upper limit (54.50 V) during the prediction horizon, and it reaches this limit at its very end.

c) Case 3 ($x(0) \in \mathcal{S}_{\text{proj}}$, $E_{\text{com}} > E_{\text{maxLG}}$): The initial state $x(0)$ is inside the polytope $\mathcal{S}_{\text{proj}}$, while commanded energy E_{com} is 900 Wh. The initial battery current is calculated as convex combination of $\mathbf{I}_{\text{maxLG}}$ and $\mathbf{I}_{\text{QP}}$ and then iterative sliding along the ellipsoid towards the maximum of $SOC(N)$ is performed to finally obtain the optimal current profile. Figure 8 shows the discharging of the battery stack due to positive values of the battery current. The algorithm successfully keeps the current of the battery stack below the maximal discharging current (206.40 A) provided by the manufacturer. The battery SOC is approaching the lower limit at the end of the prediction horizon. Additionally, the battery voltage reaches the lower limit (42.00 V) at the last minute.

d) Case 4 ($x(0) \notin \mathcal{S}_{\text{proj}}$, $E_{\text{com}} < E_{\text{CH}}$): The initial state $x(0)$ is not inside the polytope $\mathcal{S}_{\text{proj}}$, while commanded energy E_{com} is -460 Wh. The initial battery current is calculated as convex combination of $\mathbf{I}_{\text{SLP}}$ and $\mathbf{I}_{\text{CH}}$ and then iterative

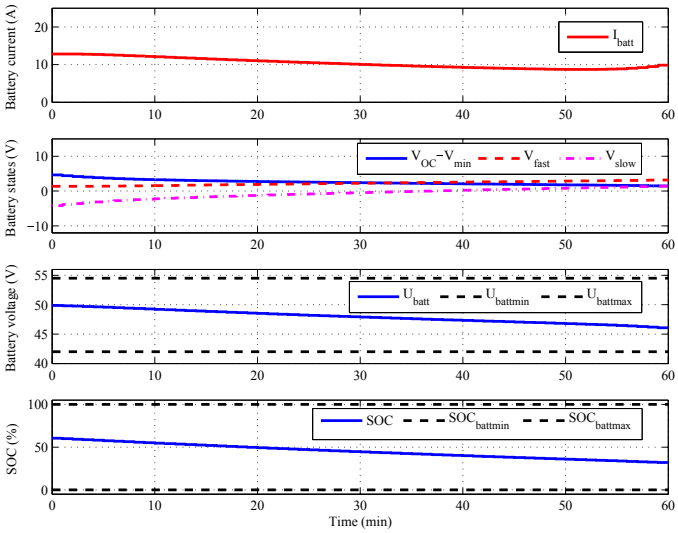

Fig. 6. Analysis of Case 1: Prediction of the battery behaviour during T_{MGR} = 60 min - $x(0) \in \mathcal{S}_{\mathrm{proj}}$, $E_{\mathrm{com}} \in [E_{\mathrm{minLG}}, E_{\mathrm{maxLG}}]$, E_{com} = 500 Wh

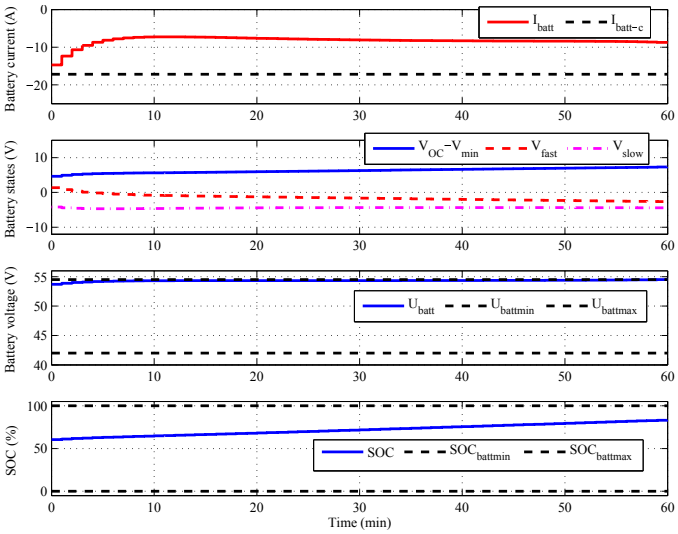

Fig. 7. Analysis of Case 2: Prediction of the battery behaviour during T_{MGR} = 60 min - $x(0) \in \mathcal{S}_{\mathrm{proj}}$, $E_{\mathrm{com}} < E_{\mathrm{minLG}}$, E_{com} = -450 Wh

sliding along the ellipsoid towards the maximum of $SOC(N)$ is performed to finally obtain the optimal current profile. Figure 9 shows the discharging of the battery stack with high current in order to retain the battery voltage under the upper limit (54.50 V). As shown, during the discharging which lasts three minutes, the open-circuit voltage decreases. After that, the algorithm charges the battery stack for the rest of the prediction time in order to achieve the commanded energy, while the open-circuit voltage, the battery voltage and the SOC increase. During the charging the algorithm keeps the current values below the maximal charging current (17.20 A).

e) Case 5 ($x(0) \notin \mathcal{S}_{\mathrm{proj}}$, $E_{\mathrm{com}} \geq E_{\mathrm{CH}}$): The initial state $x(0)$ is not inside the polytope $\mathcal{S}_{\mathrm{proj}}$, while the commanded energy E_{com} is 900 Wh. The initial battery current is calculated as convex combination of $\mathbf{I}_{\mathrm{CH}}$ and $\mathbf{I}_{\mathrm{QP}}$ and then iterative sliding along the ellipsoid towards the maximum of $SOC(N)$ is performed to finally obtain the optimal current profile. Figure 10 shows the discharging of the battery stack, all current values are positive and the algorithm keeps them below the maximal discharging current (206.40 A). Furthermore, the battery voltage and SOC are within the upper and lower limits during the whole hour. Additionally, the battery voltage reaches the lower limit (42.00 V) at the last minute.

The computations for all cases are performed in Matlab using the mathematical programming solver CPLEX on PC (Core i5 processor, 6 GB RAM). Considering the runtime for all cases are fast (Tab. III), it can be concluded that this algorithm is applicable for online implementation.

Violation of the battery constraints does not happen when the proposed algorithm is used. The algorithm keeps the battery current, voltage and SOC within the safe limits and is thus effective in reducing battery degradation effects and prolonging the battery lifetime. It takes care that the energy flow command issued by the microgrid is exactly respected and that the energy is delivered or stored with maximum efficiency which is achieved with the maximized SOC at the end of the prediction interval.

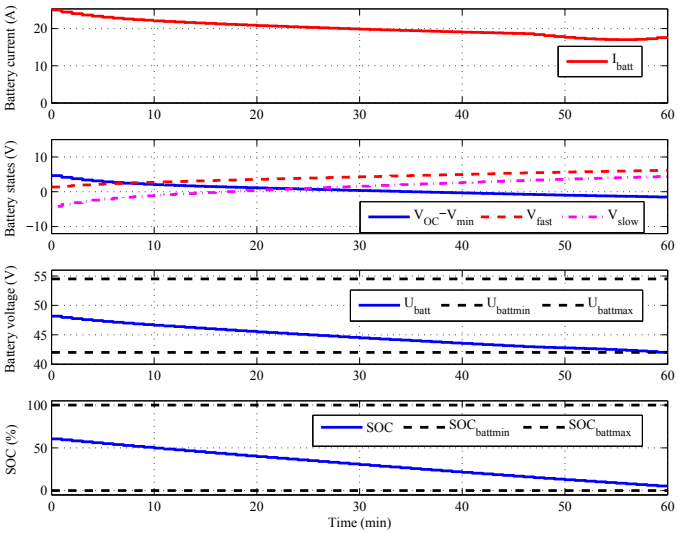

Fig. 8. Analysis of Case 3: Prediction of the battery behaviour during T_{MGR} = 60 min - $x(0) \in \mathcal{S}_{\mathrm{proj}}$, $E_{\mathrm{com}} > E_{\mathrm{maxLG}}$, E_{com} = 900 Wh

TABLE III
THE CURRENT PROFILE COMPUTATION AND THE COMPLETE OPEN-LOOP ANALYSIS RUNTIME

Simulation	Runtime
Case 1	0.0445 s
Case 2	0.5619 s
Case 3	0.3939 s
Case 4	0.6804 s
Case 5	0.9121 s

B. Simulation and experimental results of closed-loop control

In the sequel, simulation and experimental results of the closed-loop control for charging and discharging of the battery stack with the different initial conditions and set energy

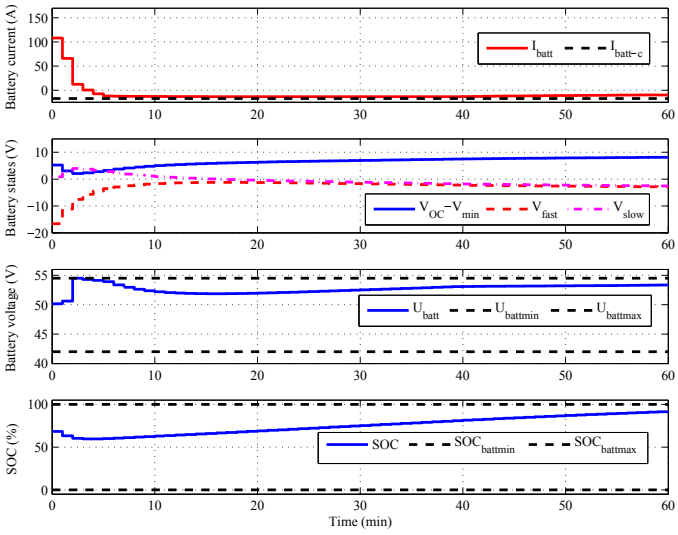

Fig. 9. Analysis of Case 4: Prediction of the battery behaviour during $T_{\mathrm{MGR}} = 60$ min - $x(0) \notin \mathcal{S}_{\mathrm{proj}}$, $E_{\mathrm{com}} < E_{\mathrm{CH}}$, E_{com} = -460 Wh

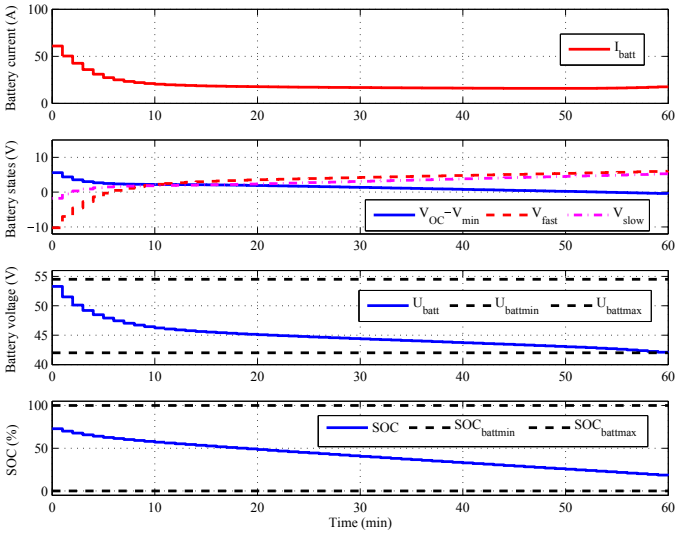

Fig. 10. Analysis of Case 5: Prediction of the battery behaviour during $T_{\mathrm{MGR}} = 60$ min - $x(0) \notin \mathcal{S}_{\mathrm{proj}}$, $E_{\mathrm{com}} \geq E_{\mathrm{CH}}$, E_{com} = 900 Wh

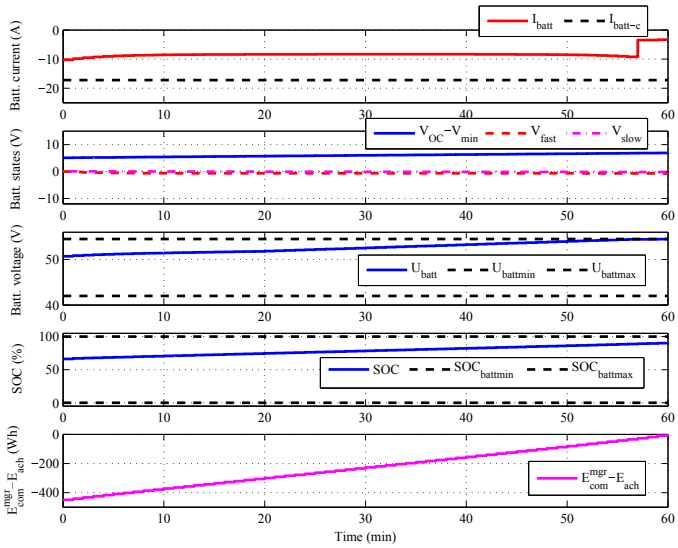

Fig. 11. Simulation results: Closed-loop predictive control of the battery charging during the one-hour runtime

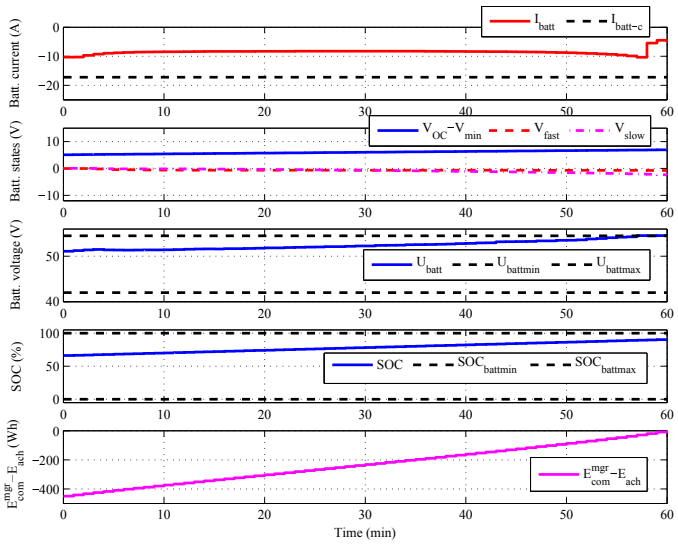

Fig. 12. Experimental results: Closed-loop predictive control of the battery charging during the one-hour runtime

exchange commands are presented. Firstly, the battery stack is charging 60 minutes with commanded energy $E_{\mathrm{com}}^{\mathrm{mgr}}$ = -450 Wh. The current state is estimated at each sampling time instant iT using the Sigma-point Kalman filter (SPKF) which is completely described in [46] for battery states and parameters estimation. In this case the estimated initial state before the testing period has started is $x(0) = [49.29 \;\; -0.04 \;\; 0.06]^T$. The simulation and experimental results of charging the VRLA battery stack using the closed-loop control algorithm are given in figures 11 and 12, respectively, where also the differences between the commanded and the achieved energy exchange ($E_{\mathrm{com}}^{\mathrm{mgr}} - E_{\mathrm{ach}}$) are shown. The algorithm keeps the current of the battery stack below the maximal charging current (17.20 A) and the battery SOC is not close to the upper and lower limit. Also, the battery voltage is very close to the upper limit (54.50 V) and it reaches this limit at the last minute. Furthermore, it can be concluded that the simulations and experiments exhibit similar behaviours and small differences are partly a consequence of the discrepancy between the battery model (3) and the experimental setup. Additionally, it can be seen that the commanded energy is successfully exchanged between the battery stack and the microgrid within the corresponding hour and yet with maximum efficiency which is reflected in the maximized residual SOC.

In order to show that this BMS is able to manage the discharging of the battery stack continuously with respect to the commanded energy exchanges, the discharge test which lasts 120 minutes (two hours) is preformed. Additionally, the overall commanded energy flow $E_{\mathrm{com}}^{\mathrm{mgr}}$ is different for each hour and its values are: $E_{\mathrm{com}}^{\mathrm{mgr}}$ = 300 Wh (the first hour) and $E_{\mathrm{com}}^{\mathrm{mgr}}$ = 200 Wh (the second hour). The estimated initial state before the testing period has started is $x(0) = [51.55 \;\; -0.01 \;\; -0.01]^T$. Figures 13 and 14 show the simulation and

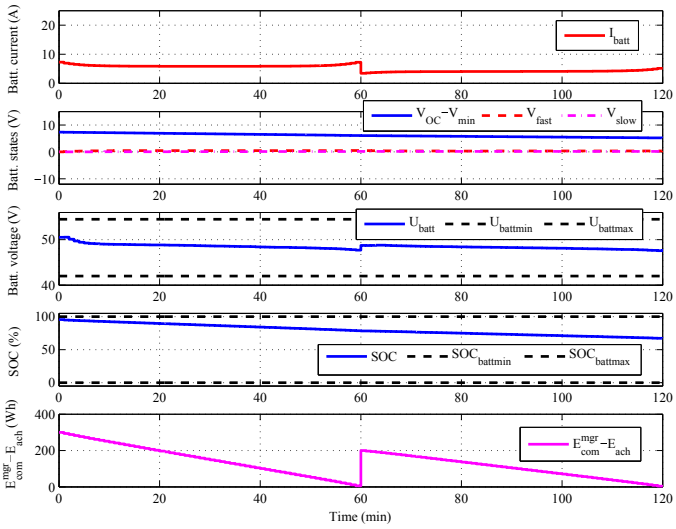

Fig. 13. Simulation results: Closed-loop predictive control of the battery discharging during the two-hour runtime

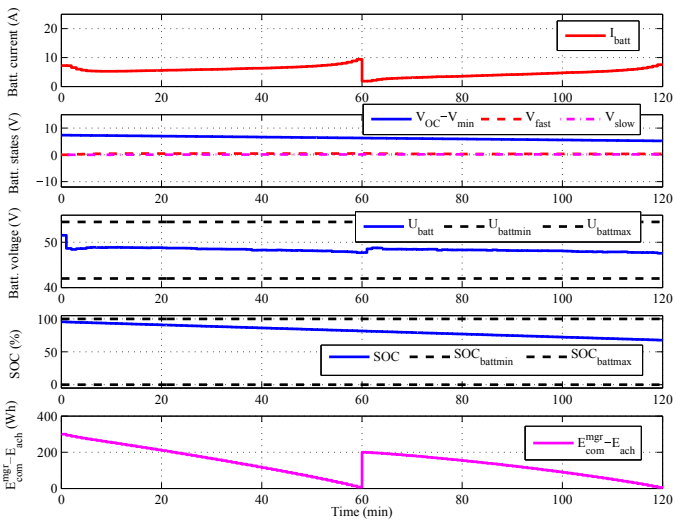

Fig. 14. Experimental results: Closed-loop predictive control of the battery discharging during the two-hour runtime

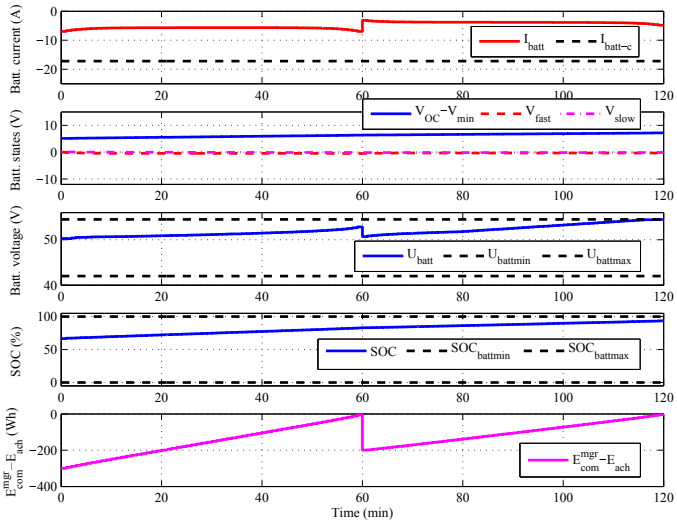

Fig. 15. Simulation results: Closed-loop predictive control of the battery charging during the two-hour runtime

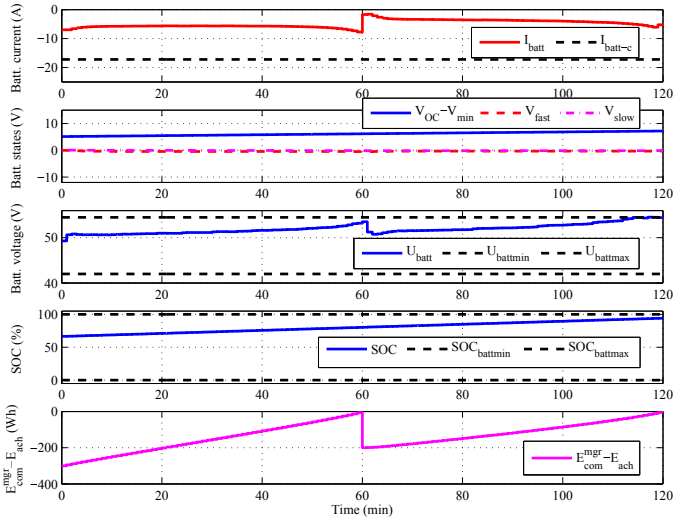

Fig. 16. Experimental results: Closed-loop predictive control of the battery charging during the two-hour runtime

experimental results, respectively. Again similar behaviours in simulation and experiment are exhibited. All current values are significantly less than the maximal discharging current ($I_{\text{batt}} \leq 206.40$ A). Further, it can be seen that all voltage and SOC values are within their allowed ranges.

After the two-hour discharging, the charging of battery stack which lasts two hours is performed. The overall commanded energy flow $E_{\text{com}}^{\text{mgr}}$ is also different for each hour and its values for the first and the second hour are: $E_{\text{com}}^{\text{mgr}}$ = -300 Wh and $E_{\text{com}}^{\text{mgr}}$ = -200 Wh, respectively. In this case the estimated initial state before the testing period has started is $x(0) = [49.32 \quad -0.03 \quad 0.04]^T$. Figures 15 and 16 show the simulation and experimental results, respectively. The battery SOC is within the upper and lower limit, while the battery voltage is very close to the upper limit (54.50 V) and it reaches this limit at the last minute.

It can be concluded that this closed-loop control algorithm successfully retains the inputs, states and outputs of the battery stack within the operational longevity constraints. Also, in all previous cases, it can be seen that the commanded energy is successfully exchanged between the battery stack and the microgrid within the corresponding hour. This control algorithm thus takes care that the energy exchange required by the microgrid level is exactly delivered or stored in given time, yet with maximum efficiency which is reflected in the maximized residual SOC.

VI. Conclusion

A new method for energy management of energy storages in microgrids is introduced that resides on model predictive control and ensures energy exchange between the storage and the rest of the microgrid is performed in exactly the commanded amount within the given time. It also ensures that all the storage longevity constraints are respected and that the

energy exchange is performed with maximum efficiency by maximizing the residual state of charge of the storage.

The approach is verified via simulations and experiments on a valve-regulated lead-acid battery storage. The effectiveness of the approach and the feasibility of real-time implementation are demonstrated through simulations and experiments.

ACKNOWLEDGMENT

This work has been supported by the Croatian Science Foundation under the project No. 6731 Control-based Hierarchical Consolidation of Large Consumers for Integration in Smart Grids (3CON) and by Interreg Danube Transnational Programme through the project Smart Building - Smart Grid - Smart City (3Smart), grant DTP1-502-3.2-3Smart.

REFERENCES

[1] L. Zhu, Z. Yan, W.-J. Lee, X. Yang, Y. Fu, and W. Cao, "Direct Load Control in Microgrids to Enhance the Performance of Integrated Resources Planning," *IEEE Transactions on Industry Applications*, vol. 51, no. 5, pp. 3553–3560, 2015.

[2] Z. Ding, W.-J. Lee, and J. Wang, "Stochastic Resource Planning Strategy to Improve the Efficiency of Microgrid Operation," *IEEE Transactions on Industry Applications*, vol. 51, no. 3, pp. 1978–1986, 2015.

[3] A. Tani, M. B. Camara, and B. Dakyo, "Energy Management in the Decentralized Generation Systems Based on Renewable Energy – Ultracapacitors and Battery to Compensate the Wind/Load Power Fluctuations," *IEEE Transactions on Industry Applications*, vol. 51, pp. 1817–1827, 2015.

[4] M. Farhadi and O. Mohammed, "Energy Storage Technologies for High-Power Applications," *IEEE Transactions on Industry Applications*, vol. 52, pp. 1953–1961, 2016.

[5] R. C. Dugan, J. A. Taylor, and D. Montenegro, "Energy Storage Modeling for Distribution Planning," *IEEE Transactions on Industry Applications*, vol. 53, pp. 954–962, 2017.

[6] T. Reddy, *Linden's Handbook of Batteries*, 4th ed. McGraw-Hill Education, 2010.

[7] D. Pavković, M. Lobrović, M. Hrgetić, and A. Komljenović, "A design of cascade control system and adaptive load compensator for battery/ultracapacitor hybrid energy storage-based direct current microgrid," *Energy Conversion and Management*, vol. 114, pp. 154–167, 2016.

[8] Y. Wong, W. Hurley, and W. Wölfle, "Charge regimes for valve-regulated lead-acid batteries: Performance overview inclusive of temperature compensation," *Journal of Power Sources*, vol. 183, no. 2, pp. 783–791, 2008.

[9] P. M. Hunter and A. H. Anbuky, "VRLA battery rapid charging under stress management," *IEEE Transactions on Industrial Electronics*, vol. 50, no. 6, pp. 1229–1237, 2003.

[10] A. Saez-de Ibarra, E. Martinez-Laserna, D. I. Stroe, M. Swierczynski, and P. Rodriguez, "Sizing Study of Second Life Li-ion Batteries for Enhancing Renewable Energy Grid Integration," *IEEE Transactions on Industry Applications*, vol. 52, pp. 4999–5008, 2016.

[11] Y. Li, P. Chattopadhyay, and A. Ray, "Dynamic data-driven identification of battery state-of-charge via symbolic analysis of input–output pairs," *Applied Energy*, vol. 155, pp. 778–790, 2015.

[12] J. P. Torreglosa, P. García-Triviño, L. M. Fernández-Ramirez, and F. Jurado, "Decentralized energy management strategy based on predictive controllers for a medium voltage direct current photovoltaic electric vehicle charging station," *Energy Conversion and Management*, vol. 108, pp. 1–13, 2016.

[13] Y. Riffonneau, S. Bacha, F. Barruel, and S. Ploix, "Optimal power flow management for grid connected PV systems with batteries," *IEEE Transactions on Sustainable Energy*, vol. 2, no. 3, pp. 309–320, 2011.

[14] Y. Levron, J. M. Guerrero, and Y. Beck, "Optimal power flow in microgrids with energy storage," *IEEE Transactions on Power Systems*, vol. 28, no. 3, pp. 3226–3234, 2013.

[15] I. N. Haq, E. Leksono, M. Iqbal, F. Sodami, D. Kurniadi, B. Yuliarto *et al.*, "Development of Battery Management System for Cell Monitoring and Protection," in *2014 International Conference on Electrical Engineering and Computer Science (ICEECS)*. IEEE, 2014, pp. 203–208.

[16] E. M. Krieger and C. B. Arnold, "Effects of undercharge and internal loss on the rate dependence of battery charge storage efficiency," *Journal of Power Sources*, vol. 210, pp. 286–291, 2012.

[17] R. Yamin and A. Rachid, "Embedded State of Charge and State of Health Estimator Based on Kalman Filter for Electric Scooter Battery Management System," in *2014 IEEE Fourth International Conference on Consumer Electronics, Berlin (ICCE-Berlin)*. IEEE, 2014, pp. 440–444.

[18] A. Bouharchouche, E. M. Berkouk, and T. Ghennam, "Control and Energy Management of a Grid Connected Hybrid Energy System PV - Wind with Battery Energy Storage for Residential Applications," in *2013 8th International Conference and Exhibition on Ecological Vehicles and Renewable Energies (EVER)*. IEEE, 2013, pp. 1–11.

[19] H. Lan, S. Wen, Y.-Y. Hong, C. Y. David, and L. Zhang, "Optimal sizing of hybrid PV/diesel/battery in ship power system," *Applied Energy*, vol. 158, pp. 26–34, 2015.

[20] A. Choudar, D. Boukhetala, S. Barkat, and J.-M. Brucke, "A local energy management of a hybrid PV-storage based distributed generation for microgrids," *Energy Conversion and Management*, vol. 90, pp. 21 – 33, 2015.

[21] E. Hittinger, T. Wiley, J. Kluza, and J. Whitacre, "Evaluating the value of batteries in microgrid electricity systems using an improved Energy Systems Model," *Energy Conversion and Management*, vol. 89, pp. 458–472, 2015.

[22] R. Dufo-López, J. M. Lujano-Rojas, and J. L. Bernal-Agustín, "Comparison of different lead–acid battery lifetime prediction models for use in simulation of stand-alone photovoltaic systems," *Applied Energy*, vol. 115, pp. 242–253, 2014.

[23] M. Vašak and G. Kujundžić, "Comparison of Battery Management Approaches for Energy Flow Optimization in Microgrids," in *17th International Conference on Power Electronics and Motion Control*. PEMC, 2016.

[24] S. S. Thale, R. G. Wandhare, and V. Agarwal, "A Novel Reconfigurable Microgrid Architecture With Renewable Energy Sources and Storage," *IEEE Transactions on Industry Applications*, vol. 51, pp. 1805–1816, 2015.

[25] H. Rahimi-Eichi, U. Ojha, F. Baronti, and M.-Y. Chow, "Battery management system: an overview of its application in the smart grid and electric vehicles," *IEEE Industrial Electronics Magazine*, vol. 7, no. 2, pp. 4–16, 2013.

[26] M. Chen and G. A. Rincon-Mora, "Accurate electrical battery model capable of predicting runtime and I–V performance," *IEEE Transactions on Energy Conversion*, vol. 21, no. 2, pp. 504–511, 2006.

[27] M. Kulkarni and V. D. Agrawal, "Energy source lifetime optimization for a digital system through power management," in *2011 IEEE 43rd Southeastern Symposium on System Theory (SSST)*. IEEE, 2011, pp. 73–78.

[28] G. Kujundžić, Š. Ileš, J. Matuško, and M. Vašak, "Optimal charging of valve-regulated lead-acid batteries based on model predictive control," *Applied Energy*, vol. 187, pp. 189–202, 2017.

[29] T. Dragičević, "Hierarchical control of a direct current microgrid with energy storage systems in a distributed topology," Ph.D. dissertation, Faculty of Electrical Engineering and Computing, University of Zagreb, 2013.

[30] B. S. Bhangu, P. Bentley, D. A. Stone, and C. M. Bingham, "Nonlinear observers for predicting state-of-charge and state-of-health of lead-acid batteries for hybrid-electric vehicles," *IEEE Transactions on Vehicular Technology*, vol. 54, no. 3, pp. 783–794, 2005.

[31] P. T. Krein and R. S. Balog, "Life extension through charge equalization of lead-acid batteries," in *2002. INTELEC. 24th Annual International Telecommunications Energy Conference*. IEEE, 2002, pp. 516–523.

[32] P. M. Hunter, "VRLA battery float charge: analysis and optimisation," Ph.D. dissertation, University of Canterbury, Christchurch, New Zealand, 2003.

[33] D. A. J. Parker, P. T. Moseley, J. Garche, and C. D. Parker, "Valve-Regulated Lead-Acid Batteries." Amsterdam: Elsevier, 2004.

[34] D. Berndt, "Valve-regulated lead-acid batteries," *Journal of Power Sources*, vol. 100, no. 1, pp. 29–46, 2001.

[35] D. P. Bertsekas, "Constrained optimization and lagrange multiplier methods," *Athena Scientific*, 1999.

[36] ——, "Nonlinear programming," *Athena Scientific, Belmont, Massachusetts*, 1999.

[37] F. Blanchini, "Set invariance in control," *Automatica*, vol. 35, no. 11, pp. 1747–1767, 1999.

[38] L. Rodrigues, "Stability analysis of piecewise-affine systems using controlled invariant sets," *Systems & control letters*, vol. 53, no. 2, pp. 157–169, 2004.

[39] M. Vašak, "Time Optimal Control of Piecewise Affine Systems," Ph.D. dissertation, Faculty of Electrical Engineering and Computing, University of Zagreb, 2007.
[40] M. Baotić, "Optimal Control of Piecewise Affine Systems–a Multi-parametric Approach–," Ph.D. dissertation, ETH Zürich, 2005.
[41] D. Q. Mayne, J. B. Rawlings, C. V. Rao, and P. O. Scokaert, "Constrained model predictive control: Stability and optimality," *Automatica*, vol. 36, no. 6, pp. 789–814, 2000.
[42] Ritar, "RA 12-45," *http://www.nps.com.au/wp-content/uploads/2013/10/RA12-45.pdf, [Online; accessed 10-December-2015]*, no. 1.
[43] "IBM ILOG CPLEX, Optimization Studio CPLEX User's Manual," *IBM Corporation, 1987*, vol. Version 12, Release 6, 2014.
[44] G. Kujundžić, M. Vašak, and J. Matuško, "Estimation of VRLA Battery States and Parameters using Sigma-point Kalman Filter," in *International Conference on Electrical drives and power electronics (18; 2015); Joint Slovak-Croatian Conference (7; 2015)*, 2015.
[45] M. Herceg, M. Kvasnica, C. Jones, and M. Morari, "Multi-parametric toolbox 3.0," in *Proceedings of the European control conference*, no. EPFL-CONF-186265, 2013.
[46] G. L. Plett, "Sigma-point Kalman filtering for battery management systems of LiPB-based HEV battery packs: Part 2: Simultaneous state and parameter estimation," *Journal of Power Sources*, vol. 161, no. 2, pp. 1369–1384, 2006.

Mario Vašak is a full professor at the Department of Control and Computer Engineering, University of Zagreb Faculty of Electrical Engineering and Computing and he is heading its Laboratory for Renewable Energy Systems. His research interests are in the domain of dynamic systems predictive control with applications to systems from the low-carbon energy sector. He is the main inventor of the US patent for fault-tolerant control of wind turbine generators and has designed the concept of hierarchical and modular energy management in buildings with integrated microgrids for enabling their economically optimal interoperation. He authored more than 15 papers in international scientific journals and overall more than 100 internationally reviewed papers. He served as president of Control Systems Chapter of the IEEE Croatia Section in period 2014-2017.

Goran Kujundžić received the Dipl.Ing. and Ph.D. degrees from University of Zagreb Faculty of Electrical Engineering and Computing, Croatia in 2000 and 2017 respectively. Currently he is employed at the Public Enterprise Croatian Telecom JSC Mostar in Power Distribution Division where he worked as a Designer and Project Manager. His main field of scientific interest is control and management of energy storage systems in microgrids that are based on renewable energy sources. He is the author or co-author of several scientific and professional papers in the field of energy storage systems, renewable energy sources and management of energy storage systems in microgrids. He is the member of the international professional organization IEEE.